Internally Controlled and Dynamic Optical Measures of Functional Tumor Biology

Taemoon Chung, Libia Garcia, Manojit M. Swamynathan, Fieke E. M. Froeling, Lloyd C. Trotman, David A. Tuveson, and Scott K. Lyons*

Cite This: *Anal. Chem.* 2023, 95, 5661−5670

Read Online

ACCESS | Metrics & More | Article Recommendations | Supporting Information

ABSTRACT: Imaging defined aspects of functional tumor biology with bioluminescent reporter transgenes is a popular approach in preclinical drug development as it is sensitive, relatively high-throughput and low cost. However, the lack of internal controls subject functional bioluminescence to a number of unpredictable variables that reduce this powerful tool to semi-quantitative interpretation of large-scale effects. Here, we report the generation of sensitive and quantitative live reporters for two key measures of functional cancer biology and pharmacologic stress: the cell cycle and oxidative stress. We developed a two-colored readout, where two independent enzymes convert a common imaging substrate into spectrally distinguishable light. The signal intensity of one color is dependent upon the biological state, whereas the other color is constitutively expressed. The ratio of emitted colored light corrects the functional signal for independent procedural variables, substantially improving the robustness and interpretation of relatively low-fold changes in functional signal intensity after drug treatment. The application of these readouts in vitro is highly advantageous, as peak cell response to therapy can now be readily visualized for single or combination treatments and not simply assessed at an arbitrary and destructive timepoint. Spectral imaging in vivo can be challenging, but we also present evidence to show that the reporters can work in this context as well. Collectively, the development and validation of these internally controlled reporters allow researchers to robustly and dynamically visualize tumor cell biology in response to treatment. Given the prevalence of bioluminescence imaging, this presents significant and much needed opportunities for preclinical therapeutic development.
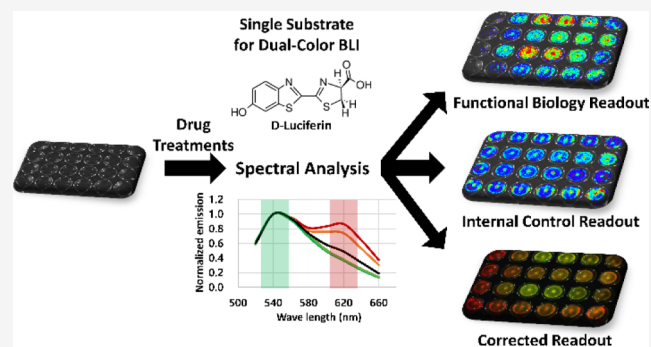
INTRODUCTION

Bioluminescence imaging (BLI) with firefly luciferase is a popular approach in preclinical oncology and is frequently used to dynamically measure relative tumor cell viability in vitro or in vivo.[1−4] Its non-destructive nature allows tumor cells to be repeatedly measured over time in the same tissue culture sample or individual subject (e.g., before and after drug treatment). BLI has a large dynamic range, and when employed in this manner it is not uncommon for the signal intensity to change by several orders of magnitude over the course of an experiment. As an optical approach, BLI is not considered truly quantitative, but background imaging noise is low, and these large changes in signal intensity over time can be meaningfully interpreted to reflect relative change in viable tumor burden.

Numerous examples also exist in the literature that describe creative transgenic strategies to restrict luciferase expression to a defined biological state.[5−7] In this way, levels of bioluminescence can be used as a proxy indicator of functional biology and are therefore a powerful research tool to non-destructively assess the specific effects of experimental genetic

or pharmacologic perturbations. Such functional bioluminescence measures can be significantly more challenging to interpret, however, as the difference in signal intensity pre- and post-experimental perturbation is often only several fold. Moreover, light output can be affected by multiple other factors unrelated to the biological measure, especially after the administration of a therapeutic. Between images, administered cancer drugs may reduce viable cell number, alter cellular metabolism, or modulate drug efflux pump expression (and consequently substrate bioavailability).[8,9] Tumor hypoxia, pH,[10] temperature (in vitro),[11] or depth in tissue (in vivo)[12] also affect light output. Moreover, a gain of functional bioluminescent signal is preferable, as signal loss can occur for technical reasons unrelated to the biology of interest.
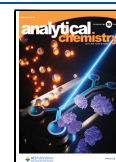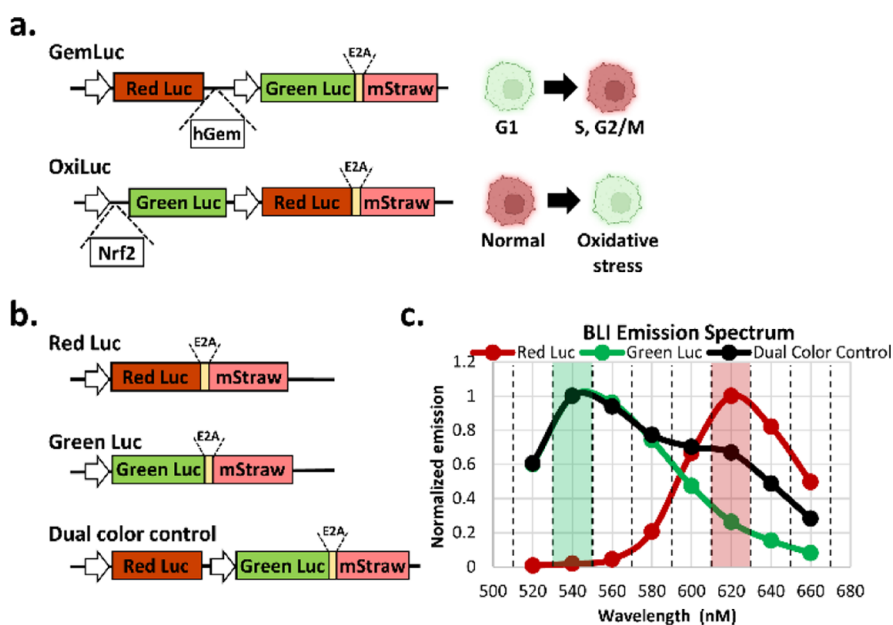
Figure 1. (a) Transgenic organization of the internally controlled cell cycle readout (GemLuc) and OS readout (OxiLuc). (b) Transgenic organization of both the single-color control and dual-color control vectors. (c) Graph depicting the spectral emission of green- and red-only control vectors in vitro (normalized to their peak emissions at 540 and 620 nm, respectively), as well as the dual color control vector for reference. The dashed lines show the 20 nm bandwidth filters employed to acquire spectral emission.

To best address these issues and achieve robust and non-destructive measures of biological state, we describe here the development of two new and internally controlled bio-luminescent indicators of functional tumor cell stress. Termed GemLuc and OxiLuc, these dual-color indicators confer non-destructive and corrected bioluminescent readouts of the cell cycle and oxidative stress (OS), respectively. We employ spectrally distinguishable green and red luciferase enzymes in these vectors, click beetle green (CBG99) and *Photinus pyralis* red-emitting luciferase 9 (PRE9).[13,14] The protein stability of one color changes according to biology, whereas the other color is constitutively expressed and always on, acting crucially as an internal control to standardize and better interpret changes in the intensity of the functional measure. Both bioluminescent enzymes utilize the same imaging substrate (D-luciferin), allowing correction of the functional signal for any variation in substrate bioavailability between images. Expression of the functional color is regulated at the post-translational level in both vectors, so they confer a fast response to experimental perturbation. A gain or loss of functional color relative to the constitutive expression of the internal control is now also of equal experimental relevance.

We present data here showing the application and validation of both internally controlled readouts to robustly and non-destructively measure cycling cells or the induction of OS, as well as providing methodology for their correct use. To maximize ease of use, we have built both colored enzymes into a single lentiviral vector to deliver the stable expression of either imaging readout via a single cell transduction event. Our approach is versatile and readily customizable to other internally controlled readouts of functional biology or bioluminescent enzymes.

■ EXPERIMENTAL SECTION

GemLuc and OxiLuc Plasmid Construction. All gene expression constructs were built into the pBOB lentiviral backbone (third generation lentiviral vector[15]). Reporter genes [CBG99 (Green Luc), PRE9 (Red Luc), and mStrawberry (mStraw)], protein degron sequences, additional genetic elements (e.g., E2A sequence[16]), and useful flanking restriction sites were all synthesized from GenScript USA (New Jersey) and assembled as finished vectors (as shown in Figures 1 and S1) within 1 to 3 restriction enzyme or Gibson Assembly cloning steps. All restriction enzymes, T4 DNA ligase, taq DNA polymerase, and the Gibson cloning kit were supplied by NEB. All plasmids were grown in Top10 competent bacteria (Invitrogen, Waltham, MA), and plasmid DNA was prepped from bacteria with Qiagen DNA mini- or maxi-prep kits (Germantown, MD).

Single-Color Control Plasmids. Single-color red or green lentiviral vectors were built to generate reference spectra for subsequent spectral unmixing. Lentiviral vectors contained either CBG99-E2A-mStrawberry or PRE9-E2A-mStrawberry expression cassettes, transcribed from a constitutive CBH (short-form CAGS) promoter (see Figure 1b).

In Vitro Cell Culture, Lentiviral Packaging, and Reporter Labeling. HEK293T cells (ATCC, Manassas, VA) and MIA PaCa-2 cells (human pancreatic cancer; ATCC, Manassas, VA) were maintained in Dulbecco's modified Eagle's medium (Corning, Lowell, MA) supplemented with 10% fetal bovine serum (Corning, Lowell, MA) and penicillin–streptomycin (Corning, Lowell, MA). All cells were grown at 37 °C and 5% CO_2 in a humidified incubator and tested negative for mycoplasma using the MycoAlert Mycoplasma Detection Kit (LT07-318, Lonza, Morristown, NJ).

Lentivirus was produced by transfection of HEK293T packaging cells with three packaging plasmids[30] (pMDL, pRSV-REV, and pCMV-VSVG) and the lentiviral reporter plasmid using Lipofectamine 3000 (Invitrogen, Waltham, MA) according to the manufacturer's recommended protocol. The supernatant containing lentivirus was then collected 72 h later, aliquoted and stored at −80 °C.

MIA PaCa-2 cells were seeded on a 6-well plate (Corning, Glendale, AZ) at a density of 3×10^5 cells/well and transduced with 500 μL lentiviral supernatant plus polybrene (MilliporeSigma, Burlington, MA) to a final concentration of 8 μg/mL. Transduced cells were then expanded further in culture and FACS sorted for mStrawberry expression (BD-FACS Aria, BD Bioscience, Franklin Lakes, NJ).

Spectral Bioluminescence Imaging and Drug Treatment In Vitro. All bioluminescence images were acquired on an IVIS Spectrum scanner (PerkinElmer, MA). Spectral bioluminescence images of live cells growing in vitro were acquired 2 min after adding 150 μg/mL of D-luciferin (Goldbio, Saint Louis, MO). Sequential images were acquired through optical filters ranging from 520 to 660 nm at 20 nm intervals, using the Spectral Unmixing option in the Imaging Wizard of Living Imaging software 4.0 (PerkinElmer, MA). For GemLuc and cell cycle imaging, exposure times were 10 s for each filter. For OxiLuc and OS imaging, to compensate for low levels of green light, 60 s images were acquired from 520 to 580 nm optical filters, then 30 s from 600 to 660 nm. All in vitro images were acquired at field of view C and focused at 0.5 cm subject height. Photon flux from each well was quantified as photons/second/steradian/cm^2 with Living Image Software 4.0 (PerkinElmer, MA). A spectral unmixing algorithm within Living Image, trained with our single-color reference spectra, was then applied to better discriminate the bioluminescent light from CBG99 (green) or PRE9 (red) enzymes.

For cell cycle imaging, 3×10^5 MIA PaCa-2/GemLuc cells were either plated day −1 on a black-walled 6-well plate (Cellvis, Mountain View, CA) or a clear bottom 6-well plate (Corning, Glendale, AZ). Bioluminescence spectra were then acquired after treatment with cisplatin or ribociclib (Selleckchem, Radnor, PA), as indicated in the main text. For dynamic imaging of the cell cycle, 5×10^4 MIA PaCa-2/GemLuc cells were seeded on a black-walled 24-well plate (Cellvis, Mountain View, CA) and treated with 10 μM of RO-3306 (CDK1 inhibitor; Sigma, Burlington, MA) for 24 h. The culture medium was then refreshed and the plate imaged as indicated in the main text.

For OS imaging, 5×10^4 or 8×10^3 MIA PaCa-2/OxiLuc cells were plated day −1 on a black-walled 24-well plate or 96-well plate (Cellvis, Mountain View, CA). Bioluminescence spectra were then acquired after Vitamin K3 (VK3) and N-acetylcysteine (NAC) treatment (both MiliporeSigma, Burlington, MA) or auranofin and buthionine sulfoximine (both Sigma, Burlington, MA) treatment, or BBI-608 (Boston Biomedical, Cambridge, MA) and Dicoumarol (Selleckchem, Radnor, PA) treatment, as indicated in the main text.

Flow Cytometry. To quantifiably analyze the cell cycle readout, treated cells were harvested at defined experimental time points and fixed with 2% formaldehyde in PBS for 15 min at room temperature. Fixed cells were then washed with PBS and stained with 3 μM DAPI (Thermo Scientific, Waltham, MA). Cells were then analyzed with a FACSAria flow cytometer (BD Bioscience, Franklin Lakes, NJ) to determine the proportion of cells in G1 or S, G2, M phases of the cell cycle.

Quantitative RT-PCR. Total RNA was extracted from tumor cells (before or after drug treatment) with TRIzol reagent (Invitrogen, Waltham, MA). cDNA was then synthesized using 1 mg of total RNA and M-MLV reverse transcriptase according to the manufacturer's instructions (Invitrogen, Waltham, MA). Quantitative PCR was then

performed at 95 °C for an initial 3 min, followed by 40 cycles of denaturation at 95 °C for 15 s, annealing and extension at 60 °C for 60 s using gene-specific TaqMan primer and TaqMan Universal Master Mix (Applied Biosystems, San Francisco, CA) on a QuantStudio 6-flex real-time PCR instrument (Applied Biosystems, San Francisco, CA). Quantification of relative gene expression was performed with the QuantStudio real-time PCR software v1.1 (Applied Biosystems, San Francisco, CA) and normalized to actin expression levels.

Quantification of Glutathione. The GSH/GSSG ratios were quantified using the GSH/GSSG-Glo assay kit (Promega, Madison, WI) to measure intracellular OS. To measure the total glutathione or GSSG of the cell, each sample was tested in 96-well culture plates with total glutathione or GSSG lysis reagent. 5 min after adding the lysis reagent, the luciferin generation reagent and detection reagents were added. Plates were then read in a SpectraMax microplate reader (Molecular devices, San Jose, CA).

In Vivo Tumor Models and In Vivo Spectral Bioluminescence Imaging. All procedures were conducted in accordance with the IACUC at Cold Spring Harbor Laboratory, and all mice were housed in a temperature- and humidity-controlled vivarium on a 12 h dark−light cycle with free access to food and water.

All in vivo studies employed either male NSG (NOD.Cg Prkdc^{scid}Il2rg^{tm1Wji}/SzJ) or nude mice (Balb/c Foxn1^{nu}/Foxn1^{nu}), aged between 6 and 8 weeks (JAX Laboratory, Bar Harbor, ME). All in vivo BLI was conducted with an IVIS Spectrum scanner.

To establish tumors, 1×10^6 MIA PaCa-2 cells [expressing GemLuc or OxiLuc (or single color controls to train spectral unmixing)] were engrafted subcutaneously. Once tumors had visibly developed (≥ 5 mm in diameter), mice were spectrally imaged and treated with cancer therapies as indicated in the main text. Briefly, mice were anesthetized with 2% isoflurane and injected I.P. with 300 mg/kg of D-luciferin. Anesthesia was maintained, and spectral images were acquired starting at 15 min after the injection. As per in vitro spectral imaging, sequential images were acquired through optical filters ranging from 520 to 660 nm at 20 nm intervals, using the spectral unmixing option in the Imaging Wizard of Living Imaging software 4.0. Exposure time per filter was 10 s or 60 s for cell cycle imaging or OS imaging, respectively, using field of view D and focused at 1.5 cm subject height. All images were analyzed with Living image software 4.0, and a spectral unmixing algorithm within Living Image, trained with our in vivo single-color reference spectra, was then applied to better discriminate emitted light from CBG99 (green) or PRE9 (red) enzymes. The signal intensity of emitted light was quantified as photons/second/steradian/cm^2.

To induce OS in vivo, 10 mg/kg of sodium arsenite (ASN; Sigma, Burlington, MA) or PBS control was injected intraperitoneally. All mice were spectrally imaged immediately before and 5 h after ASN treatment.

Statistical Analysis. Statistical analyses were performed using R Statistical Software (version 4.0.4; R Foundation for Statistical Computing, Vienna, Austria), Graphpad Prism 5(GraphPad software, Inc, La Jolla, CA), and Microsoft Excel (Redmond, WA). The p-value less than 0.05, 0.01, and 0.001, mentioned as *, **, and ***, respectively, are considered as statistically significant.
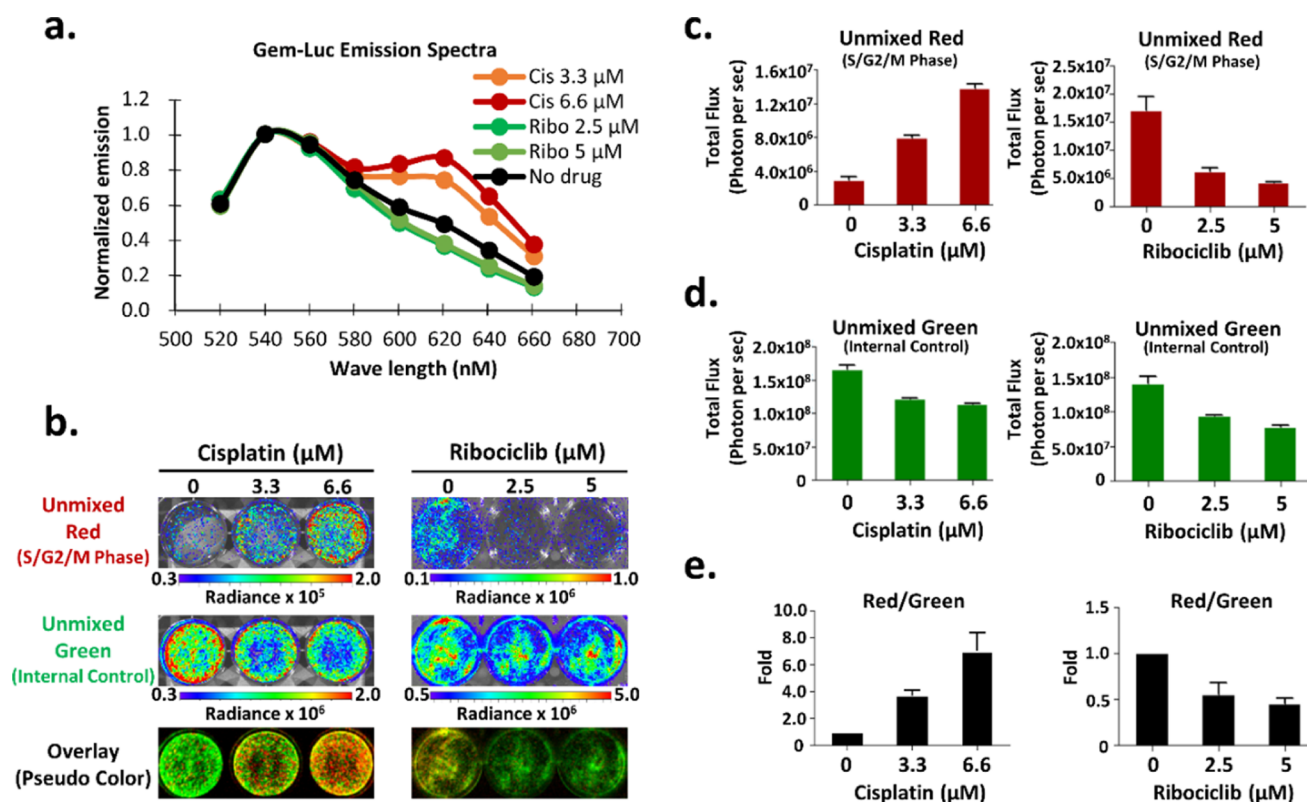
Figure 2. Non-destructive and internally controlled readouts of treatment effects on the cell cycle (GemLuc). (a) Normalized spectral emission of GemLuc-expressing MIA PaCa-2 cells growing in vitro, 48 h after drug treatment with either cisplatin or ribociclib. Spectra normalized to peak emission at 540 nm. (b) Representative spectrally unmixed red and green images (and pseudo-color overlay) of GemLuc expressing MIA PaCa-2 cells growing in vitro, 48 h after drug treatment. (c,d) Show measurement of functional red and internal-control green light after spectral unmixing and show both dose-dependent drug effects to the cell cycle and viable cell number. (e) Ratio of measured red/green light corrects for experimental variables and produces a robust measure of cell cycle effects. Results show the mean ± SD of three technical replicates in one experiment.

RESULTS

GemLuc and OxiLuc Vector Construction. To facilitate the introduction of the internally controlled cell cycle (GemLuc) or OS (OxiLuc) readouts into a cell line of interest, each was built into a single lentiviral vector. As shown in Figures 1a and S1, both green luciferase (CBG99) and red luciferase (PRE9) expression cassettes are constitutively transcribed from two independent promoters.

To make GemLuc report cycling cells (cell cycle), we fused the Geminin degron (amino acids 1−110 of the human Geminin protein) to the C-terminus of the red luciferase. This is the same peptide degron sequence employed in the original fluorescent FUCCI vector[17] and confers protein stability (and red bioluminescence) only at proliferative phases (S, G2, and M) of the cell cycle. The red luciferase is otherwise ubiquitinated and degraded by the proteasome at the non-proliferative G1 phase of the cell cycle. Relative to the "always on" green enzyme, however, the presence or absence of red bioluminescence is meaningful, so the construct enables internally controlled measures of both proliferative and non-proliferative phases of the cell cycle.

The green enzyme (CBG99) is approximately 3-fold brighter than the red enzyme (PRE9), and in an effort to boost OxiLuc imaging sensitivity, we reversed these colors such that the green enzyme is the functional color and red the internal control. We fused the NRF2 degron (Neh 2,4,5 domains)[18,19] to the N-terminus of the green enzyme. This conferred continuous proteasomal degradation of the green enzyme in "normal" cell conditions in a Keap1-dependent manner, but protein stabilization and an increase in green light relative to the red internal control in the presence of OS. In both GemLuc and OxiLuc constructs, we positioned an E2A-mStrawberry cassette in-frame with the constitutively expressed internal control enzyme. This added the ability to sort stably transduced cells for red fluorescence by flow cytometry or to directly visualize transduced cells by fluorescence microscopy.

Single-Color Controls for Spectral Unmixing. There is considerable spectral overlap between the bioluminescent emissions of CBG99 and PRE9 (Figure 1b). Accordingly, we used optical filters and a spectral unmixing algorithm[20] to best discriminate functional from control signals. To generate green or red only reference spectra and enable unmixing, we built constitutively expressed single-color lentiviral vectors (Figure 1b). Both of these constitutively expressed either a PRE9-2A-mStrawberry or a CBG99-2A-mStrawberry cassette from a constitutive promoter (CBH; short-form CAGGS).[21] Polyclonal stably transduced populations of MIA PaCa-2 cells for each color were then generated by flow sorting for strong fluorescence. Reference in vitro red and green bioluminescence spectra were then acquired by imaging these cells across a range of 20 nm bandpass optical filters with an IVIS Spectrum scanner (PerkinElmer). Encouragingly, the fold ratio of measured and spectrally unmixed red to green bioluminescence reflected the mixture of plated colored cells (Figure S2).

Non-destructive and Internally Controlled Readouts of Treatment Effects on the Cell Cycle (GemLuc). To
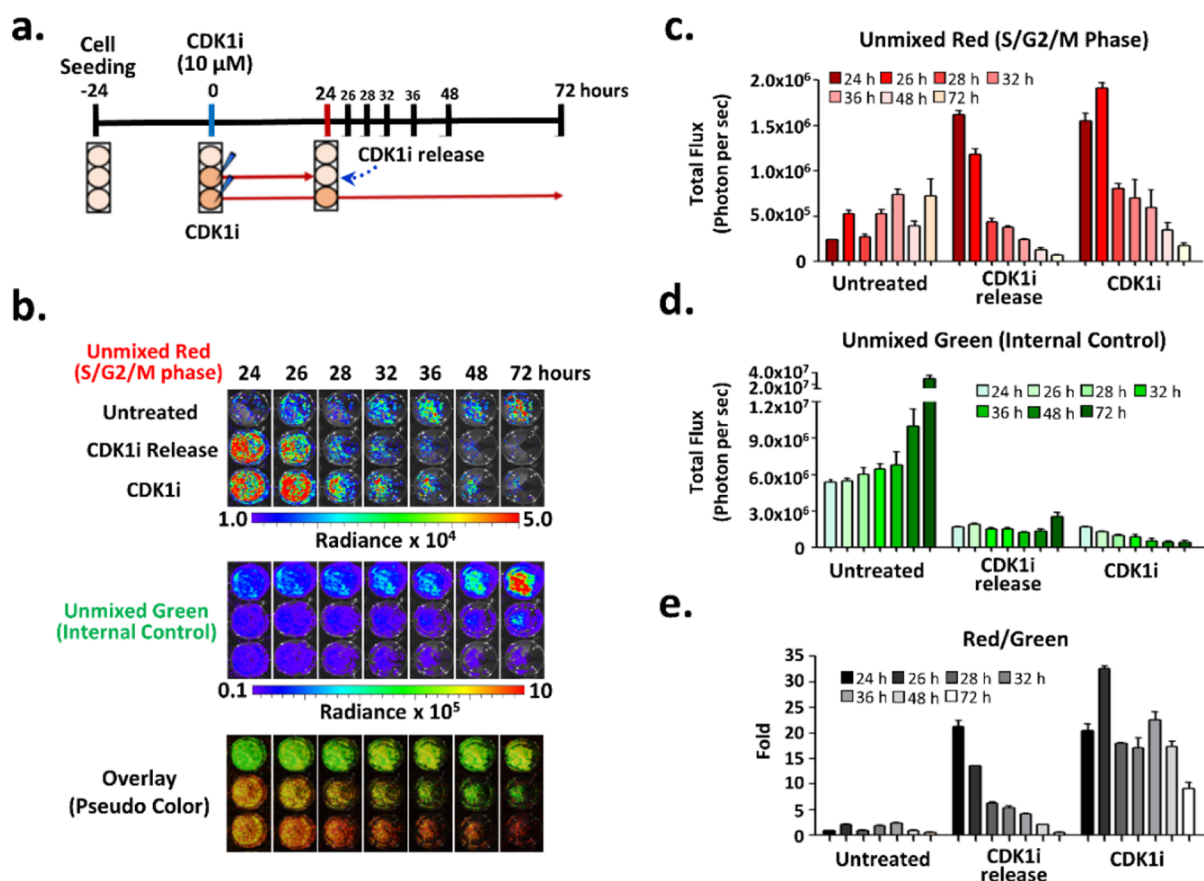
Figure 3. Imaging cell cycle dynamics. (a) Schematic overview of the experiment treatment of MIA PaCa-2/GemLuc cells with the CDK1 inhibitor, RO3306. (b) Shows spectrally unmixed or pseudo-colored images of cells in the three experimental conditions, control untreated, 10 μM RO3306 treated for 24 h, then refreshed in regular tissue culture media, or 10 μM RO3306 treated for 72 h. (c,d) Show spectrally unmixed measurements of functional red and internal-control green light, taken at regular timepoints over 72 h. (e) Ratio of measured red/green light corrects the functional cell cycle readout and differentiates the cause of signal loss between differences in the proportion of cells in cycle versus viable cell number after treatment. Results show the mean ± SD of three technical replicates in one experiment.

demonstrate the ability of GemLuc to indicate both proliferative and non-proliferative phases of the cell cycle, we added escalating doses of cisplatin (predicted S/G2 phase arrest[22]) or ribociclib (predicted G1/S phase arrest[23]) to GemLuc expressing MIA PaCa-2 cells in vitro and spectrally imaged 48 h later. The results are shown in Figure 2 and demonstrate that, relative to expression of the internal control, GemLuc is able to non-destructively indicate the accumulation of cells in proliferative or non-proliferative phases of the cell cycle. Note that both chemotherapeutic treatments are partially cytotoxic and cause a decrease in the signal intensity of the internal control (green light) in a dose-dependent manner. In contrast, we observed that the functional red signals increased after cisplatin treatment and decreased after ribociclib treatment. By taking the ratio of red to green light, we use the internal control to account for decreased viable cell number and correct the functional red signal, making the cell cycle measure more accurate. Flow cytometry of treated cells in repeated experiments validated the optical readout by showing comparable shifts of cells within different phases of the cell cycle after treatment (shown in Figure S3).

Visualizing Cell Cycle Dynamics and Synchronization after Treatment. Our internally controlled functional biology readouts are non-destructive and thus enable dynamic measures over an extended period of time after experimental perturbation. This is illustrated in Figure 3, where GemLuc-

labeled MIA PaCa-2 cells were treated in vitro with the CDK1 inhibitor RO3306.[24] 24 h after treatment and an evident cell cycle arrest at G2/M, one well was refreshed with normal media. These "released" cells are subsequently seen to progress synchronously into the G1 phase of the cell cycle. Without an internal control to this measure, the loss of functional signal could have been attributed to the cytotoxic effects of the drug, but normalization of the red functional signal with the green internal control corrects for this, and we robustly see that surviving cells are synchronously entering a non-proliferative phase of the cell cycle. Maintenance of the drug over this same time period was seen to perpetuate the G2/M arrest and give rise to a significant drop in cell viability at later experimental timepoints.

Non-destructive and Internally Controlled Readouts of Treatment-Induced OS (OxiLuc). In parallel with the Gem-Luc experiments, we also tested the performance of the OxiLuc reporter for its ability to report physiologically relevant levels of OS (i.e., intracellular ROS levels that stabilize Nrf2). The colors are reversed in this vector, and the induction of OS is indicated by an increase in green light. As shown in Figure 4, we treated MIA PaCa-2-OxiLuc cells with escalating doses of VK3 (menadione), which is well known to induce ROS.[25] The fast response of our degron-based imaging readout was really exemplified in this study, as we were able to measure a dramatic fold induction of the functional green color just 2 h
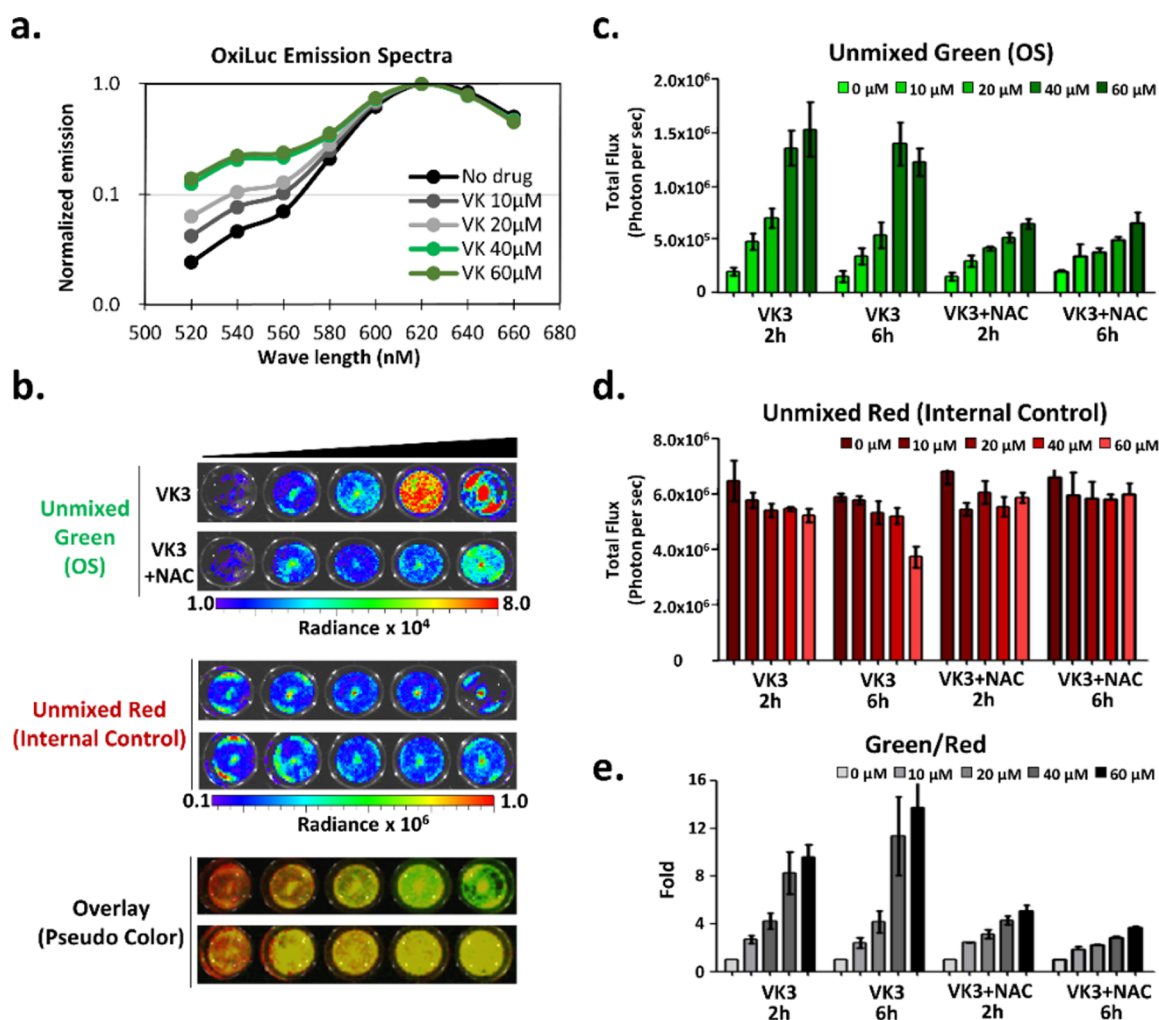
Figure 4. Non-destructive and internally controlled readouts of treatment effects on the generation of OS (OxiLuc). (a) Shows normalized spectral emissions of OxiLuc expressing MIA PaCa-2 cells growing in vitro on the same plate, 6 h after drug treatment with increasing concentrations of vitamin K3 (menadione). Spectra normalized to peak emission at 620 nm. (b) Representative spectrally unmixed red and green images (and pseudo-color overlay) of OxiLuc-expressing MIA PaCa-2 cells growing in vitro, 6 h after treatment with VK3 or VK3 and NAC. (c,d) Show measurement of functional green (OS) and internal-control red light after spectral unmixing and show dose-dependent drug effects on the generation of OS (as early as 2 h after treatment) and minimal effects on cell viability. (e) Ratio of measured green/red light corrects for experimental variables and produces a robust measure of treatment effects on the induction of OS. Results show the mean ± SD of three technical replicates in one experiment.

after administration of the drug. The intensity of the control color was only a little affected as drug concentration increased over this short time period, resulting in minimal correction of the functional signal. Significantly, however, we could substantially reduce both the induction of green light and the cytotoxicity of higher doses by repeating the experiment in the presence of the antioxidant NAC, indicating that the experimental observations are predominantly ROS- dependent. We further confirmed OS dependency by quantifying levels of HMOX-1 by qRT-PCR and the GSH/GSSG ratio on treated cell lysates (see Figure S4). Similarly, we observed a robust induction of OS following the treatment of MIA PaCa-2-OxiLuc-cells after treatment with the investigational drug napabucasin (BBI-608)[26] (Figure S5). Our in vitro imaging approach is amenable to relatively high throughput analysis and so can be useful in investigating the biological effects conferred by combination treatments. As shown in Figure 5, we plated out OxiLuc-expressing cells in a 6 by 6 grid on a 96-well plate format and varied the concentrations of auranofin

(Aur) along the *y*-axis and buthionine sulphoximine (BSO) along the *x*-axis. We observed minimal induction of OS with either drug alone. However, image analysis showed that the addition of even relatively low doses of BSO can potentiate the induction of OS in combination with doses of Aur above 100 nM.

In Vivo Imaging of Functional Biology. BLI is particularly well-suited to making sensitive non-invasive in vivo measurements. However, spectral BLI in vivo can be challenging and is complicated by the fact that green light is significantly less transmissible through tissue than red light.[27] We therefore reasoned that labeled tumors should develop at both a superficial and fixed body location to maximize in vivo performance. Accordingly, we established single-color reference spectra from subcutaneous tumors to allow spectral unmixing in future experiments (see Figure S6). We then conducted two key control experiments to show that the internal control can broadly correct the functional color for two important in vivo experimental variables. To demonstrate
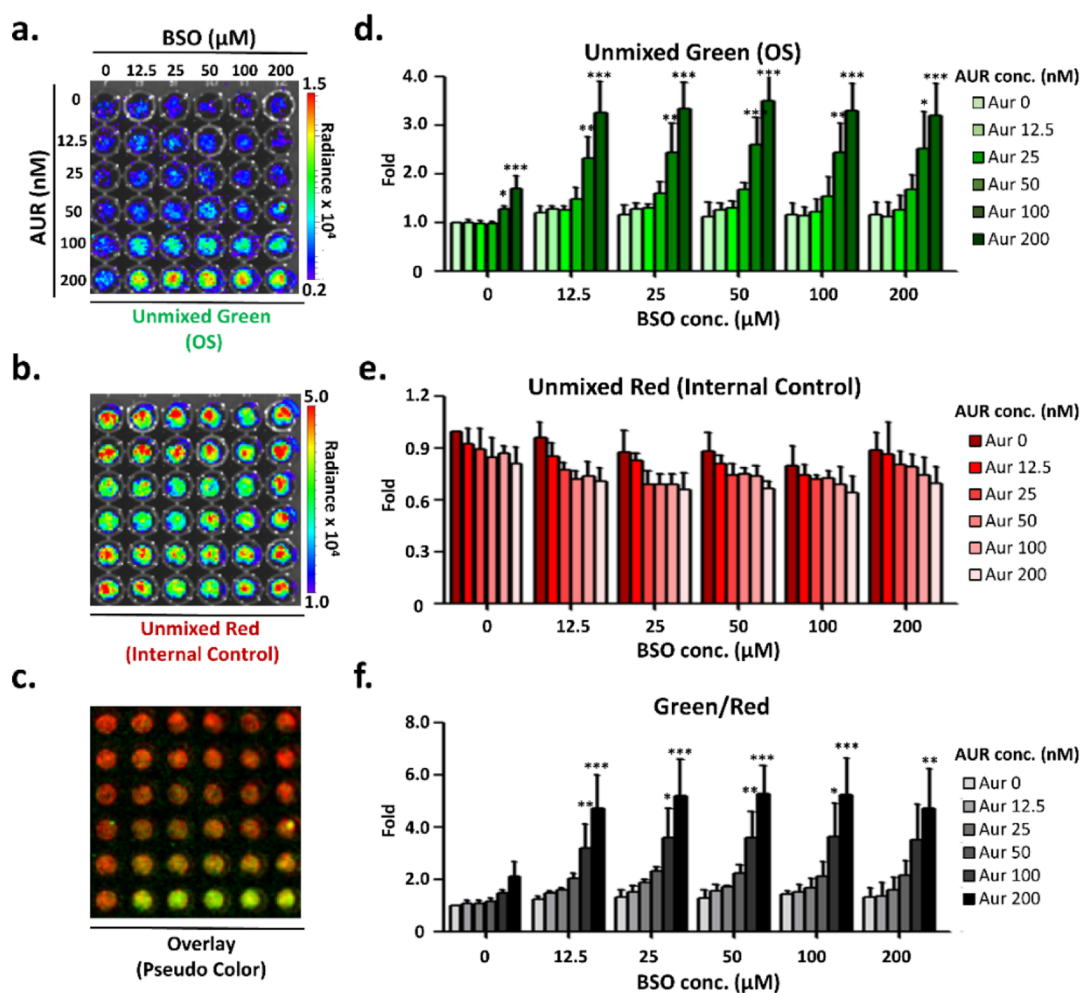
Figure 5. Imaging synergistic drug effects on the induction of OS. (a−c) Spectrally unmixed red and green images (and pseudo-color overlay) of OxiLuc-expressing MIA PaCa-2 cells in vitro, plated out on a 96-well format, 24 h after treatment with increasing concentrations of Aur (top to bottom of plate) and BSO (left to right of plate). (d) Spectrally unmixed green light was quantified following combination drug treatments (increased green light indicative of OS). (e) Spectrally unmixed red light (internal control) was quantified in parallel to correct the functional measure for experimental variables. (f) Green/red fold ratio for a robust non-destructive measure of OS induction. Results show the mean ± SD of three independent experiments. The significance of differences between the groups were compared to the baseline for each BSO concentration using ANOVA, followed by pairwise comparisons using Welch's two-sample t-test. P-values were adjusted for multiple comparisons by Dunnett's method. The p-value less than 0.05, 0.01, and 0.001, mentioned as *, **, and ***, respectively.

correction of the functional measure for differences in viable tumor cell number between images, we set up five mice with subcutaneous GemLuc-expressing MIA PaCa-2 tumors and spectrally imaged them at regular time intervals over an 18 day period (Figure S7). Without an internal control, the intensity of the functional color increased more than 40-fold as the tumors grew in size and cellularity increased, but it is not possible to attribute this signal increase to a proportionate increase of cells in S, G2, and M. The functional cell cycle measure could largely be corrected by the internal control color, however, suggesting a relatively consistent proliferative rate over this extended period of time. To show that the internal control could also correct the functional signal for variable substrate bioavailability in vivo, we took repeated spectral measures of GemLuc-expressing tumors for 2 h after a single substrate injection, as signal intensity slowly decreased to baseline levels. Those changes in bioluminescence intensity over time are primarily dependent on substrate bioavailability. As shown in Figure S8, we essentially observe those dynamic changes to functional color intensity, but again, those are not

related to the proportion of proliferating cells. Once corrected by the internal control color, we see relatively steady-state light output from the functional color over this extended period of time, irrespective of substrate bioavailability.

To demonstrate the ability of OxiLuc to image the induction of OS in vivo following the administration of a drug (see Figure 6), we implanted six mice with subcutaneous OxiLuc expressing MIA PaCa-2 tumors. Once tumors had visibly developed, we separated all mice into two cohorts: one treated with ASN to induce OS[28] and the other vehicle control. Based on in vitro observations, mice were spectrally imaged before and 5 h after treatment.

The results of this experiment were encouraging; measurement of the functional green color alone showed little evidence of an increase following treatment with OS-inducing ASN relative to untreated tumors. However, light emission from the internal control red enzyme was markedly decreased in treated mice, and so when the ratio of green to red light was made, ASN treated mice showed an induction of OS, which was
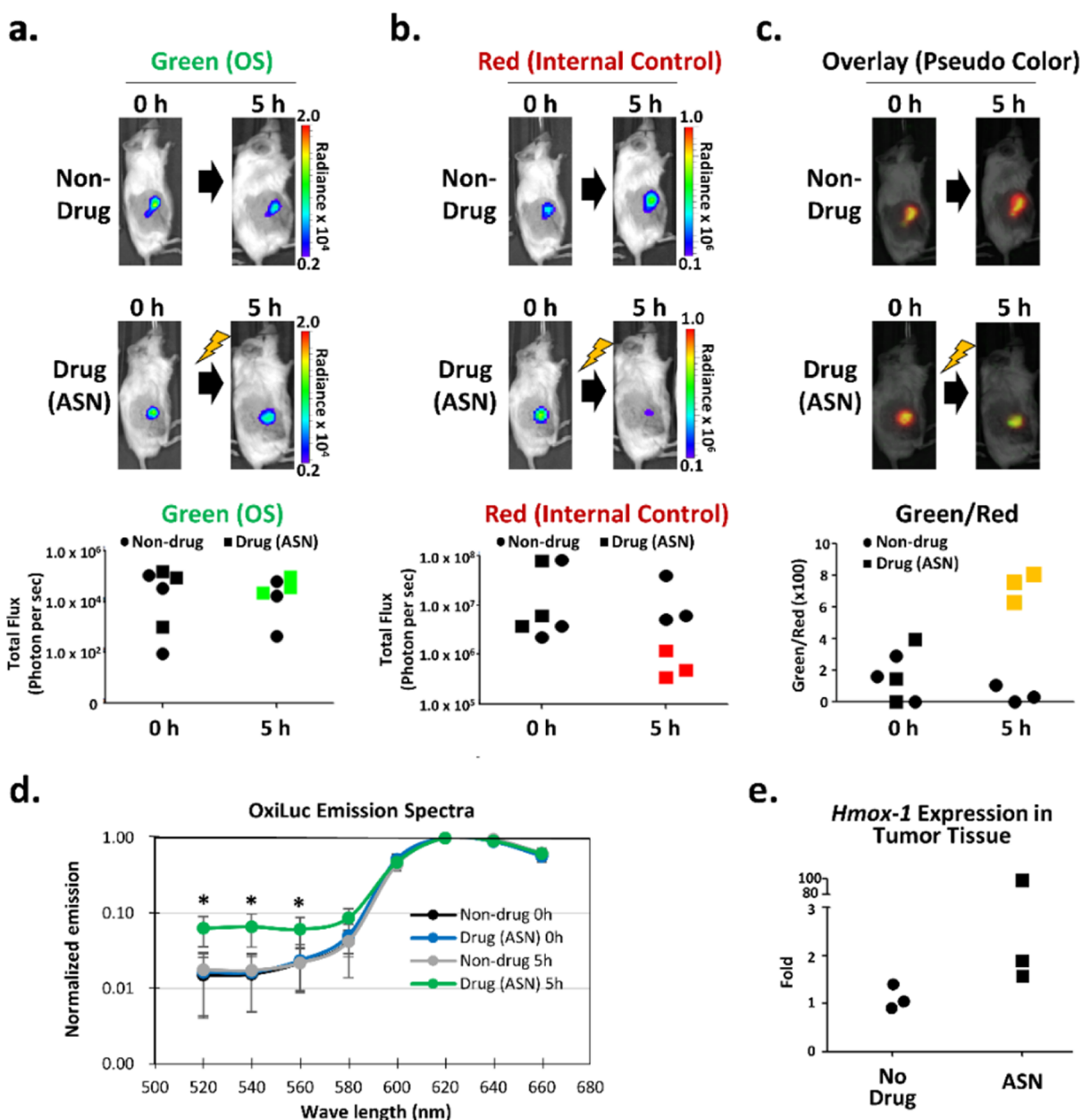
Figure 6. Imaging the induction of OS in vivo. (a) Representative image of spectrally unmixed green light (indicative of OS) before (0 h) and 5 h (5 h) after treatment with sodium arsenite or vehicle. (b) Spectrally unmixed red light (internal control) taken at the same timepoints and (c) pseudo-color overlay showing that ASN-treated tumors (■) have a significantly higher-fold increase in the ratio of green to red light than the saline-treated group (●) at this 5 h timepoint (**$p < 0.01$). The colored squares (green, red, and yellow) indicate the color of light being analyzed from drug-treated mice. A two-sided Student's *t*-test was used to identify the difference between groups. (d) Spectral emission (normalized to 620 nm) from both experimental cohorts, before and after treatment. Two-way ANOVA was used to identify the difference between groups. (*$p < 0.05$). (e) Results of qRT-PCR analysis on -*Hmox* expression to validate the induction of OS in treated mice at this single 5 h timepoint.

confirmed by analysis of HMOX 1 RNA expression levels by qRT-PCR.

DISCUSSION

Bioluminescence is frequently employed in preclinical research and drug development as a means to non-destructively measure dynamic aspects of functional tumor biology. However, given the number of non-specific variables that can substantially influence light output, it can be challenging to confidently interpret low-fold changes in signal intensity following pertubation. Cancer therapeutics are intended to exert tumor-specific cell stress and death, which in turn likely

have effects on cellular metabolism and the tumor micro-environment, all of which can have unpredictable effects on signal output unrelated to the functional biological measure. This was dramatically illustrated in two classic papers that showed that certain cancer treatments affect the expression levels of the ABCG2 drug efflux pump,[8] (or *P*-glycoprotein for coelenterazine metabolizing enzymes[29]), which in turn affect intracellular substrate levels and give rise to surprising shifts in bioluminescence intensity post-treatment.

In an effort to greatly improve the robustness of functional bioluminescence measures, which unarguably have an important role to play in preclinical research and drug

development, we report here the construction of two dual-color and internally controlled readouts of functional biology. Named GemLuc and OxiLuc (for detection of changes in the cell cycle or in levels of OS, respectively), the functional signal is corrected from substantial experimental variability by a constitutively expressed control color that metabolizes the same substrate. Others have previously described the application of two or more spectrally distinct bioluminescent colors to simultaneously image multiple independent biological parameters in mouse models.[14,30,31] Although technically impressive, none of the multi-parametric measures are internally controlled, and so the signal from each one is potentially prone to influence from any of the various factors that affect light production.

Unlike the well-defined and spectrally tight light emission typical of fluorophores, the emission wavelengths of CBG99 and PRE9 are broad and overlap considerably. Consequently, we generated single-color reference spectra to facilitate spectral unmixing and best attribute emitted photons to either colored enzyme. Both GemLuc and OxiLuc vectors are relatively modular, however, and it should be straightforward to employ different colored enzymes with alternative imaging characteristics or different regulatory elements for alternative functional biology readouts.

The in vitro application and dynamic nature of these readouts are straightforward and highly advantageous experimentally. Without imaging, it is common for researchers to choose a single or small number of arbitrary timepoints after treatment (e.g., at 24 h) to assess drug effects. These new internally controlled readouts of proliferation or OS now confer robust and temporal pharmacodynamic measures, amenable to moderately high throughput (96-well format), allowing the researcher to better visualize both how and when a cell responds to single or combination treatment prior to recovering or succumbing to cell death. As the stability of the functional color is regulated at the post-translational level in both vectors, we can observe fast responses to treatment (e.g., OS within 2 h).

In vivo imaging of colored light is complicated by the differential transmission properties of red and green light through tissue. However, we determined that tumors developing at a fixed and relatively superficial body location could be effectively imaged in this way. Following in vivo demonstration that our approach broadly corrects the functional signal for two potentially major experimental variables (differences in viable cell number and substrate bioavailability between scans), we showed the importance of an internal control to appropriately interpret images of OS induction following drug treatment of OxiLuc expressing tumors. Sodium arsenite is well-known for its ability to induce ROS in vivo; however, quantitation of the functional color alone, 5 h after treatment, showed no meaningful difference in emitted light intensity between treated and untreated tumors. Quantitation of the internal control color however showed a significant decrease in light output in treated mice, and the corrected green/red light ratio could clearly differentiate the induction of OS in treated mice. We have not exhaustively tested the in vivo sensitivity of this approach, as that is highly context-dependent and subject to the model, reporter transgene expression levels and tumor-size. However, we note that in vivo imaging sensitivity may be enhanced in the future with different bioluminescent enzymes with different spectral light emission properties. With these vectors and current imaging hardware, we believe that the utility of our approach will be limited to imaging relatively superficial tumors in vivo.

It should also be noted that the measured fold change of the functional signal relative to control is not an absolute measure and is relative to the intensity of the baseline signal. For example, we have observed that, in comparison to the MIA PaCa-2 cells described here, OxiLuc-labeled SUIT-2 pancreatic cancer cells possess higher constitutive baseline levels of OS (data not shown). As a result, despite showing similarly high levels of functional bioluminescence upon the induction of OS, they exhibit a comparably lower fold induction. Similarly, you would expect a highly proliferative cell line to have a more intense baseline functional color than a slow-growing line, and so in absolute terms, a lower-fold induction after a drug-induced S/G2/M cell cycle arrest. The ability to observe robust and dynamic changes to tumor cell biology following treatment is not compromised though.

■ CONCLUSIONS

The validated internally controlled reporters described here confer robust bioluminescence measures of anti-cancer drug effect beyond routine measures of cell viability. Their non-destructive nature means that peak levels of growth arrest or OS induction can now be observed dynamically and not measured at an estimated arbitrary and destructive timepoint.

■ ASSOCIATED CONTENT

ⓈI **Supporting Information**

The Supporting Information is available free of charge at https://pubs.acs.org/doi/10.1021/acs.analchem.2c05450.

> GemLuc and OxiLuc plasmid maps; multispectral image of single color red or green luciferase in vitro and in vivo; validation of the cell cycle arrest and the intracellular ROS induction after drug treatment; correction of the functional color measure using internal control color in vivo; and the proportion of emitted light from GemLuc and OxiLuc in each optical filter (PDF)

■ AUTHOR INFORMATION

Corresponding Author

Scott K. Lyons — *Cold Spring Harbor Laboratory, Cold Spring Harbor, New York 11724, United States;* ⓞ orcid.org/0000-0003-0139-6054; Email: slyons@cshl.edu

Authors

Taemoon Chung — *Cold Spring Harbor Laboratory, Cold Spring Harbor, New York 11724, United States*

Libia Garcia — *Cold Spring Harbor Laboratory, Cold Spring Harbor, New York 11724, United States*

Manojit M. Swamynathan — *Cold Spring Harbor Laboratory, Cold Spring Harbor, New York 11724, United States; Graduate Program in Molecular and Cellular Biology, Stony Brook University, Stony Brook, New York 11794, United States*

Fieke E. M. Froeling — *Wolfson Wohl Cancer Research Centre, Institute of Cancer Sciences, University of Glasgow, Glasgow G61 1BD, U.K.; Cancer Research UK Beatson Institute, Glasgow G61 1BD, U.K.*

Lloyd C. Trotman — *Cold Spring Harbor Laboratory, Cold Spring Harbor, New York 11724, United States*

David A. Tuveson − *Cold Spring Harbor Laboratory, Cold Spring Harbor, New York 11724, United States*

Complete contact information is available at:
https://pubs.acs.org/10.1021/acs.analchem.2c05450

Author Contributions

T.C. and S.K.L. conceived the study and transgenic approach. T.C. and L.G. conducted all experiments. M.M.S., F.E.M.F., and L.C.T. advised all oxidative stress experiments. L.C.T., D.A.T., and S.K.L. advised on cancer treatments and tumor model biology. All authors contributed to the writing and review of the manuscript. All authors have given approval to the final version of the manuscript.

Notes

The authors declare the following competing financial interest(s): DAT is a member of the Scientific Advisory Board and receives stock options from Leap Therapeutics, Surface Oncology, and Cygnal Therapeutics. DAT is cofounder of Mestag Therapeutics. DAT has received Sponsored Research Agreements from Fibrogen, Mestag, and ONO Therapeutics. FEMF receives institutional funding from AstraZeneca and Sierra Oncology (for investigator initiation clinical trial). All other authors have no COI to declare.

■ REFERENCES

(1) Lyons, S. K. *Cancer J.* **2015**, *21*, 152−164.

(2) Mezzanotte, L.; van 't Root, M.; Karatas, H.; Goun, E. A.; Löwik, C. *Trends Biotechnol.* **2017**, *35*, 640−652.

(3) Liu, S.; Su, Y.; Lin, M. Z.; Ronald, J. A. *ACS Chem. Biol.* **2021**, *16*, 2707−2718.

(4) Alsawaftah, N.; Farooq, A.; Dhou, S.; Majdalawieh, A. F. *IEEE Rev. Biomed. Eng.* **2021**, *14*, 307−326.

(5) Moroz, E.; Carlin, S.; Dyomina, K.; Burke, S.; Thaler, H. T.; Blasberg, R.; Serganova, I. *PLoS One* **2009**, *4*, No. e5077.

(6) Burd, C. E.; Sorrentino, J. A.; Clark, K. S.; Darr, D. B.; Krishnamurthy, J.; Deal, A. M.; Bardeesy, N.; Castrillon, D. H.; Beach, D. H.; Sharpless, N. E. *Cell* **2013**, *152*, 340−351.

(7) Iwawaki, T.; Akai, R.; Toyoshima, T.; Takeda, N.; Ishikawa, T. O.; Yamamura, K. I. *Sci. Rep.* **2017**, *7*, 46230.

(8) Zhang, Y.; Bressler, J. P.; Neal, J.; Lal, B.; Bhang, H. E.; Laterra, J.; Pomper, M. G. *Cancer Res.* **2007**, *67*, 9389−9397.

(9) Bakhsheshian, J.; Wei, B. R.; Chang, K. E.; Shukla, S.; Ambudkar, S. V.; Simpson, R. M.; Gottesman, M. M.; Hall, M. D. *Proc. Natl. Acad. Sci. U.S.A.* **2013**, *110*, 20801−20806.

(10) Khalil, A. A.; Jameson, M. J.; Broaddus, W. C.; Lin, P. S.; Dever, S. M.; Golding, S. E.; Rosenberg, E.; Valerie, K.; Chung, T. D. *Int. J. Mol. Imaging* **2013**, *2013*, 1.

(11) Oliveira, G.; Viviani, V. R. *Photochem. Photobiol. Sci.* **2019**, *18*, 2682−2687.

(12) Rice, B. W.; Contag, C. H. *Nat. Biotechnol.* **2009**, *27*, 624−625.

(13) Branchini, B. R.; Ablamsky, D. M.; Davis, A. L.; Southworth, T. L.; Butler, B.; Fan, F.; Jathoul, A. P.; Pule, M. A. *Anal. Biochem.* **2010**, *396*, 290−297.

(14) Mezzanotte, L.; Que, I.; Kaijzel, E.; Branchini, B.; Roda, A.; Löwik, C. *PLoS One* **2011**, *6*, No. e19277.

(15) Tiscornia, G.; Singer, O.; Verma, I. M. *Nat. Protoc.* **2006**, *1*, 241−245.

(16) Szymczak-Workman, A. L.; Vignali, K. M.; Vignali, D. A. *Cold Spring Harb. Protoc.* **2012**, *2012*, 199−204.

(17) Sakaue-Sawano, A.; Kurokawa, H.; Morimura, T.; Hanyu, A.; Hama, H.; Osawa, H.; Kashiwagi, S.; Fukami, K.; Miyata, T.; Miyoshi, H.; et al. *Cell* **2008**, *132*, 487−498.

(18) Itoh, K.; Wakabayashi, N.; Katoh, Y.; Ishii, T.; O'Connor, T.; Yamamoto, M. *Genes Cells* **2003**, *8*, 379−391.

(19) Hirotsu, Y.; Katsuoka, F.; Itoh, K.; Yamamoto, M. *Genes Cells* **2011**, *16*, 406−415.

(20) Xu, H.; Rice, B. W. *J. Biomed. Opt.* **2009**, *14*, 064011.

(21) Gray, S. J.; Foti, S. B.; Schwartz, J. W.; Bachaboina, L.; Taylor-Blake, B.; Coleman, J.; Ehlers, M. D.; Zylka, M. J.; McCown, T. J.; Samulski, R. J. *Hum. Gene Ther.* **2011**, *22*, 1143−1153.

(22) Dasari, S.; Bernard Tchounwou, P. B. *Eur. J. Pharmacol.* **2014**, *740*, 364−378.

(23) Ingham, M.; Schwartz, G. K. *J. Clin. Oncol.* **2017**, *35*, 2949−2959.

(24) Vassilev, L. T.; Tovar, C.; Chen, S.; Knezevic, D.; Zhao, X.; Sun, H.; Heimbrook, D. C.; Chen, L. *Proc. Natl. Acad. Sci. U.S.A.* **2006**, *103*, 10660−10665.

(25) Criddle, D. N.; Gillies, S.; Baumgartner-Wilson, H. K.; Jaffar, M.; Chinje, E. C.; Passmore, S.; Chvanov, M.; Barrow, S.; Gerasimenko, O. V.; Tepikin, A. V.; et al. *J. Biol. Chem.* **2006**, *281*, 40485−40492.

(26) Froeling, F. E. M.; Swamynathan, M. M.; Deschênes, A.; Chio, I. I. C.; Brosnan, E.; Yao, M. A.; Alagesan, P.; Lucito, M.; Li, J.; Chang, A. Y.; et al. *Clin. Cancer Res.* **2019**, *25*, 7162−7174.

(27) Zhao, H.; Doyle, T. C.; Coquoz, O.; Kalish, F.; Rice, B. W.; Contag, C. H. *J. Biomed. Opt.* **2005**, *10*, 041210.

(28) Oikawa, D.; Akai, R.; Tokuda, M.; Iwawaki, T. *Sci. Rep.* **2012**, *2*, 229.

(29) Pichler, A.; Prior, J. L.; Piwnica-Worms, D. *Proc. Natl. Acad. Sci. U.S.A.* **2004**, *101*, 1702−1707.

(30) Kleinovink, J. W.; Mezzanotte, L.; Zambito, G.; Fransen, M. F.; Cruz, L. J.; Verbeek, J. S.; Chan, A.; Ossendorp, F.; Löwik, C. *Front. Immunol.* **2018**, *9*, 3097.

(31) Sarrion-Perdigones, A.; Chang, L.; Gonzalez, Y.; Gallego-Flores, T.; Young, D. W.; Venken, K. J. T. *Curr. Protoc. Mol. Biol.* **2020**, *131*, No. e122.